PERGAMON

International Journal of Solids and Structures 39 (2002) 19–39

INTERNATIONAL JOURNAL OF SOLIDS and STRUCTURES

www.elsevier.com/locate/ijsolstr

Failure loads of spot welds under combined opening and shear static loading conditions

S.-H. Lin [a], J. Pan [a,*], S.-R. Wu [b], T. Tyan [b], P. Wung [b]

[a] *Department of Mechanical Engineering and Applied Mechanics, 2250 G.G. Brown Laboratory, The University of Michigan, Ann Arbor, MI 48109-2125, USA*

[b] *Ford Motor Company, Dearborn, MI 48121, USA*

Received 27 February 2001; in revised form 26 July 2001

Abstract

Failure loads of spot welds are investigated under combined opening and shear static loading conditions. Square-cup specimens were used to obtain the failure loads of mild steel spot welds under a range of combined opening and shear loads. Optical micrographs of the cross-sections of spot welds before and after failure were examined to understand the failure processes under different combinations of loads. The experimental results indicate that under nearly pure opening loads, shear failure occurs in the heat affected zone along the nugget circumferential boundary. Under combined opening and shear loading conditions, necking/shear failure starts near the nugget in the stretching side of the base metal sheet. According to the experimental observations, a simple lower bound limit load analysis is conducted. The results of the lower bound limit load analysis quantitatively agree with those of the experiments. A simple closed-form equation is proposed to characterize the failure loads of spot welds under combined opening and shear static loading conditions. The failure load is expressed as a function of the tensile strength of the base metal, the nugget size, the sheet thickness, the loading angle for characterization of combined loads, and an empirical coefficient for the given welding schedule.

Keywords: Resistance spot weld; Combined loading; Plastic limit analysis; Failure criterion

1. Introduction

Resistance spot welding is one of the primary methods to join sheet metals for automotive components. A typical car or truck may have more than 2000 spot welds. Since spot welds in automotive components are subjected to complex service loading conditions, various specimens have been used to analyze fatigue lives of spot welds (e.g., Hartmann, 1958; Davidson, 1983; Radaj, 1989; Wang and Ewing, 1991; Swellam et al., 1994; Sheppard and Pan, 2001; Zhang, 2001). The static strengths of spot welds have also been investigated.

* Corresponding author. Tel.: +1-734-764-9404; fax: +1-734-647-3170.
E-mail address: jwo@umich.edu (J. Pan).

0020-7683/01/$ - see front matter
PII: S0020-7683(01)00187-1

For example, Hartmann (1958) discussed the mechanical tests of spot welds in tension–shear, direct tension, torsion and peel specimens. VandenBossche (1977) adopted a plasticity approach to examine the strength of spot welds in lap-shear specimens. Sawhill and Furr (1981) and Ewing et al. (1982) investigated the strength of spot welds in terms of the specimen geometry, welding parameter, welding schedule, base metal strength, testing speed and testing configuration. Zuniga and Sheppard (1997) examined the failure modes of spot welds in coach-peel and lap-shear specimens. Lee et al. (1998) adopted a fracture mechanics approach using the stress intensity factor K to model their experimental results on the strength of spot welds in U-tension specimens under combined tension and shear loading conditions. Wung (2001) and Wung et al. (2001) obtained and analyzed test results from lap-shear, in-plane rotation, coach-peel, normal separation, and in-plane shear tests, and proposed a failure criterion based on the experimental data of spot welds in various specimens.

In this paper, we investigate the maximum load carrying capacity of spot welds under combined opening and shear static loading conditions, and develop a failure criterion for spot welds under such loading conditions based on experimental results and plasticity theories. The failure criterion for spot welds under static loading conditions can be used as the reference for a failure criterion for spot welds under impact loading conditions. In this investigation, simple fixtures were designed to impose different combinations of opening and shear loads. Experiments of spot weld specimens of mild steel with two different thicknesses were then conducted under various combinations of opening and shear loads. Micrographs of spot welds before and after failure were obtained to understand the physical failure processes under different combined loading conditions. Based on experimental observations, a lower bound limit load analysis is performed to investigate the effects of the combination of load, the sheet metal thickness and weld nugget radius on failure. Finally, an engineering formula is proposed to characterize the load carrying capacity of spot welds with consideration of the nugget size and sheet thickness under combined opening and shear loading conditions for automotive applications.

2. Test specimen and fixture

2.1. Test specimen

In this investigation, spot welds in mild steel specimens with thicknesses of 1.0 and 1.5 mm are considered. An engineering stress–strain curve of the mild steel sheet is shown in Fig. 1. For this sheet material, the 0.2% offset yield strength is 184.6 MPa (26.78 ksi) and the ultimate tensile strength is 302.3 MPa (43.84 ksi). In the traditional lap-shear, coach-peel, cross tension, and U-tension test specimens, the shear force and bending moment give non-uniform loading conditions along the circumference of spot welds. In order to give a relatively uniform loading along the circumference of spot welds under pure opening mode conditions, a square-cup specimen was designed by Wung and Stewart (2001).

Fig. 2 shows a failed square-cup specimen of Wung and Stewart (2001) under pure opening loading conditions. The specimen is composed of two identical square cups. The two square cups were folded from sheet metals and welded at the four corners as shown to increase the cup stiffness under dominant opening loads and to give a relative uniform loading along the circumference of the spot weld. The welding schedule of the spot welds is listed in Table 1. Two wings with reinforcement welded plates were extended from two opposite sides of the cup. Fig. 3 shows a specimen mounted to a fixture set by two bolts through the specimen holes in the wings of the specimen. The reinforcement plates prevent the sheet metal near the specimen holes from local plastic deformation during loading. The four flanges of specimens provide enough stiffness so that the loads can be applied almost uniformly along the circumference of the weld nugget under pure opening loading conditions.

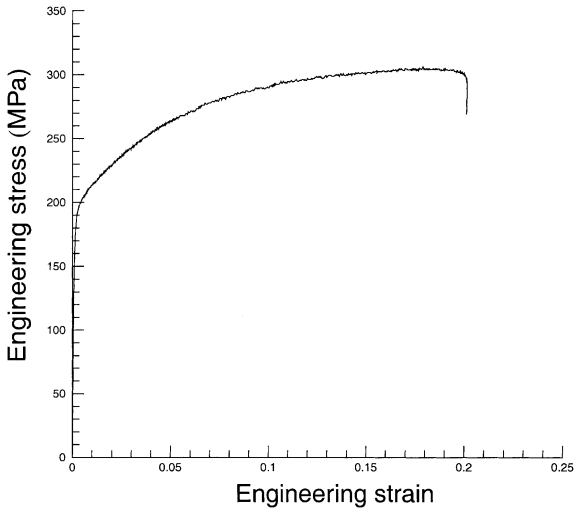

Fig. 1. An engineering stress–strain curve of mild steel sheet.

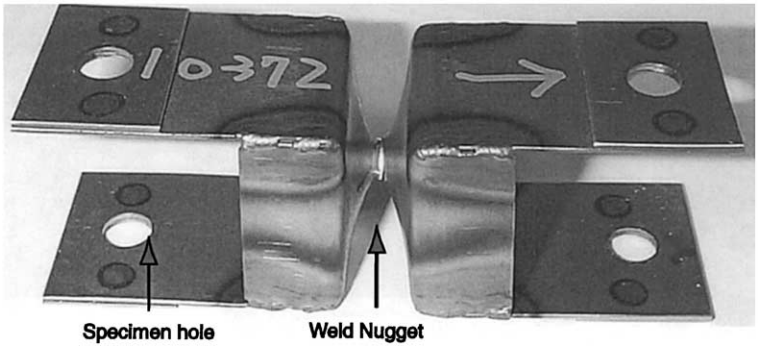

Fig. 2. A failed specimen under pure open loading conditions with a nugget pullout.

Table 1
Sheet metal weld schedule

Thickness (mm)	Minimum nugget diameter (mm)	Nominal nugget diameter (mm)	Weld time (cycles)	Weld current (kA)	Weld force (kN)
1.0	3.8	6.4	10	12.7	3.5
1.5	3.8	6.4	15	15.4	5.2

2.2. Test fixture

Four fixture sets were designed for four different combined loading conditions. One fixture set with a spot weld specimen is shown in Fig. 3. The fixture set was cut from a rectangular tube with an inclined angle as shown in Fig. 4. The inclined angle ϕ is equal to the loading angle ϕ, which represents the angle between the load application line and the centerline of specimens as shown in Fig. 4. As shown in the figure, the applied load P can be resolved into an opening load N to open the crack around the nugget circumference

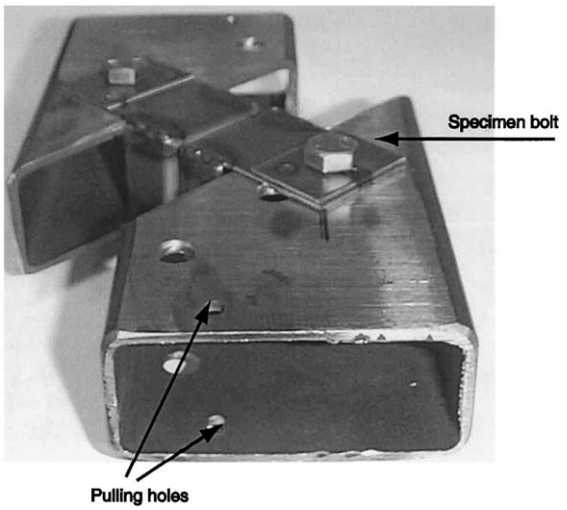

Fig. 3. A test fixture for a loading angle of 45°.

and a shear load S to shear the crack around the nugget circumference (following the fracture mechanics definition of "opening" for mode I and "shear" for mode II and III). Note that the shear load gives a combined mode from mode II to mode III around the crack front along the circumference of the nugget.

The fixture set was designed such that those two straight lines intersect at the center of the weld nugget in the specimen. Four loading angles of 0°, 22°, 45°, and 60° were considered. Fig. 3 shows a fixture set with a loading angle of 45°. Each fixture set has two specimen holes and two pulling holes. The specimens were mounted to the fixture with two bolts that passed through the specimen holes. The edges of the square cups of the specimen were designed in contact with the slanted edges of the fixture to maintain the correct loading angle during the testing as shown in Fig. 3. Meanwhile, hollow blocks cut from square tubes were inserted into the square cups of each specimen to prevent the walls of the square cups of the specimen from buckling and to keep the correct loading angle during testing.

Specimens and fixture sets were installed in a Tinius Olsen universal testing machine (a mechanical screw type tensile machine). Then a monotonically increasing displacement was applied at the rate of 12.7 mm per minute. Here, the displacement is referred to as the relative movement of point A with respective to point B as shown in Fig. 4(a). The load and displacement histories were simultaneously recorded during the testing. Tests were terminated until the two components of the specimen were almost completely separated.

3. Experimental results and failure mechanisms

Maximum loads from tests for 1.0 and 1.5 mm mild steel specimens subjected to various loading angles are listed in Table 2. The maximum loads were obtained from the load–displacement curves of the tests. Fig. 5 shows typical load–displacement curves for 1.0 mm mild steel specimens subjected to different loading angles. In general, the peak load decreases with the increasing loading angle for both 1.0 and 1.5 mm specimens. Fig. 6 shows side views of the failed 1.5 mm specimens under the loading angles of 0° and 45°. The arrows in the figure show the loading directions. Nugget pullout can be seen under pure opening loading conditions (loading angle of 0°) in Fig. 6(a). Weld nugget rotation can be seen under the loading angle of 45° in Fig. 6(b). In order to further understand the failure mechanisms, micrographs were taken

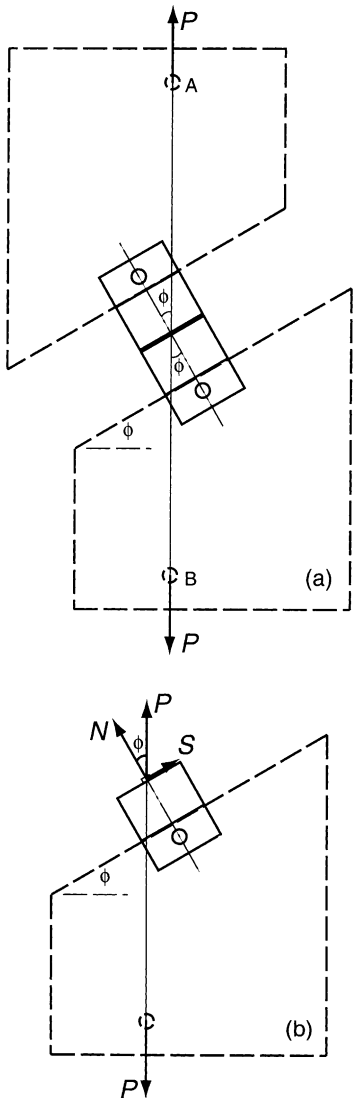

Fig. 4. (a) The applied load P is applied to the specimen with the loading angle ϕ, (b) the applied load P can be resolved into an opening load N and a shear load S.

from the cross-sections of specimens containing weld nuggets. Fig. 7 shows a micrograph of the cross-section of an undeformed spot weld from a 1.5 mm specimen. The weld nugget, heat affected zone and base metal can be seen. The notch tips near the nugget appear to be blunted with finite root radii. Fig. 8 shows a micrograph of the cross-section of a failed spot weld in a 1.5 mm specimen under opening loading conditions. The figure shows that the spot weld appears to fail only by the through thickness shear in the heat affected zone. A similar failure mechanism was also observed in coach-peel specimens of HSLA steel under static loading conditions (Zuniga and Sheppard, 1997). Fig. 9 shows a micrograph of the cross-section of a failed spot weld in a 1.0 mm specimen under pure opening loading conditions. The figure shows that the spot weld appears to fail mostly by the through thickness shear in the heat affected zone. Only a small

Table 2
Maximum loads for 1.0 and 1.5 mm mild steel specimens under various loading conditions

Run no.	Thickness of sheet metal (mm)	Loading angle (deg)	Maximum load (N)
01, 02, 03	1	0	6027, 6112, 5711
04, 05, 06	1	22	5840, 6236, 5916
07, 08, 09	1	45	5378, 5231, 5547
10, 11, 12	1	60	5729, 5409, 5796
13, 14, 15	1.5	0	9732, 8522, 9692
16, 17, 18	1.5	22	9341, 9359, 9732
19, 20, 21	1.5	45	9007, 8798, 8086
22, 23, 24	1.5	60	8714, 8242, 8353

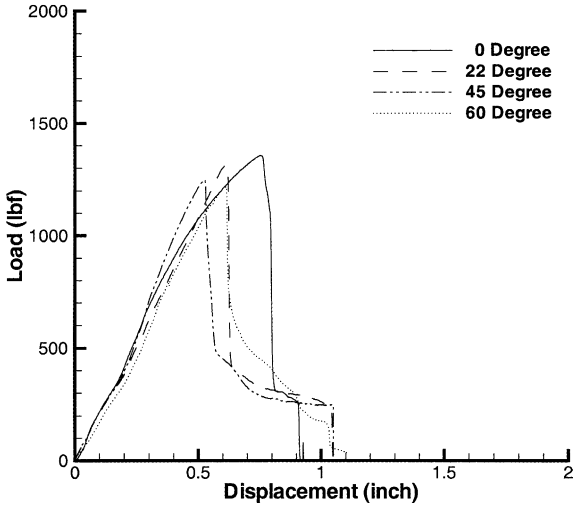

Fig. 5. Load–displacement curves for 1.0 mm mild steel specimens subjected to different loading angles.

portion of the failed spot weld appears to fail by tearing off the base metal and leaving a lip possibly due to slight misalignment during the test and non-homogeneous material properties around the weld nugget.

Fig. 10 shows a micrograph of the cross-section of a failed spot weld in a 1.5 mm specimen under combined loading conditions with a loading angle of 60°. As shown in the figure, necking due to stretching appears in the base metal near the heat affected zone in the left lower leg, as marked by leg 1. Therefore, it appears that the fracture was initiated by necking/shear in the right upper leg at point A, as marked in Fig. 10. Then the failure propagated around the circumference of the nugget (marked by B) by necking/shear. Finally, the sheet metal on the top part of the specimen was torn off and left a lip (marked by D) on the spot weld after the two square cups separated. Cracking at point C in the heat affected zone was also shown. Fig. 11 shows a micrograph of the cross-section of a failed spot weld in a 1.0 mm specimen under combined loading conditions with a loading angle of 60°. As shown in the figure, the failure mechanism is the same as that shown in Fig. 10. A similar failure mechanism is also shown in lap-shear specimens of HSLA steel under static loading conditions (Zuniga and Sheppard, 1997).

The experimental observations indicate that the failure of spot welds involves crack initiation and growth under fully plastic conditions. A detailed modeling of this complex failure process requires an expensive analytical/computational effort. Therefore, a lower bound limit load analysis is conducted here to

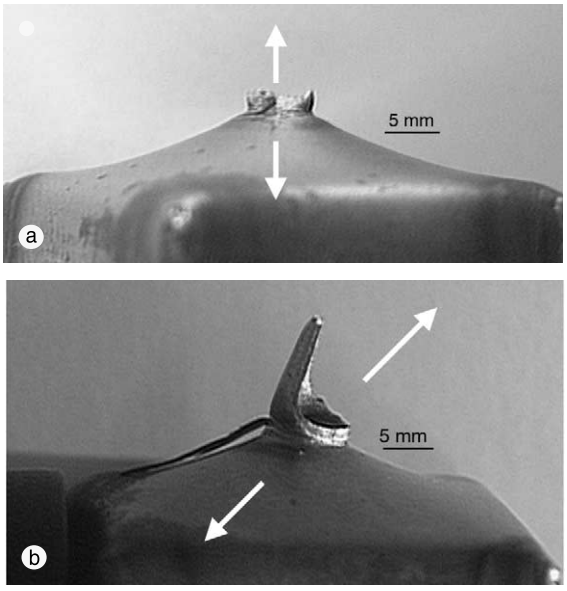

Fig. 6. Side views of failed 1.5 mm specimens under different loading angles: (a) loading angle of 0°, (b) loading angle of 45°.

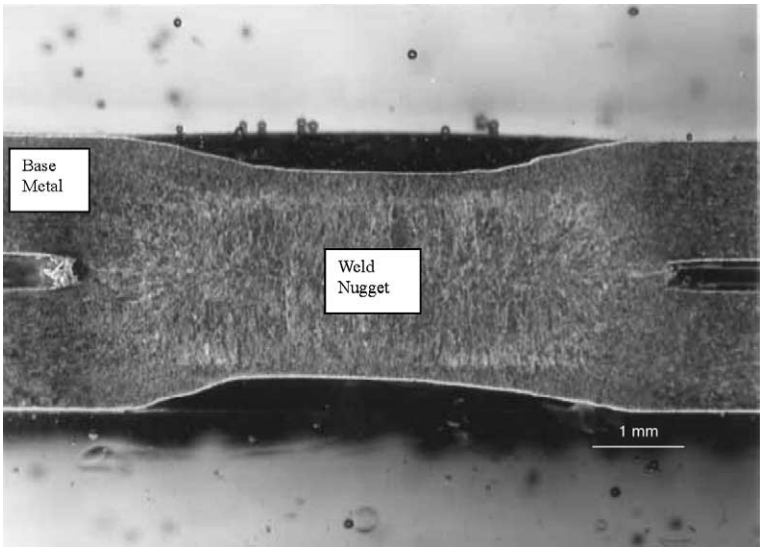

Fig. 7. A micrograph of the cross-section of a spot weld in a 1.5 mm specimen before testing. The weld nugget and base metal are all visible. The heat affected zone is between the weld nugget and base metal.

just characterize the maximum loads, or the failure loads, of spot welds. In general, the failure loads of spot welds should be expressed in terms of the loading conditions, material properties, nugget diameter, sheet thickness, and welding process parameters (Heuschkel, 1952; Sawhill and Furr, 1981). In this paper, the effects of loading conditions and sheet thickness on the maximum loads are investigated for a given nugget

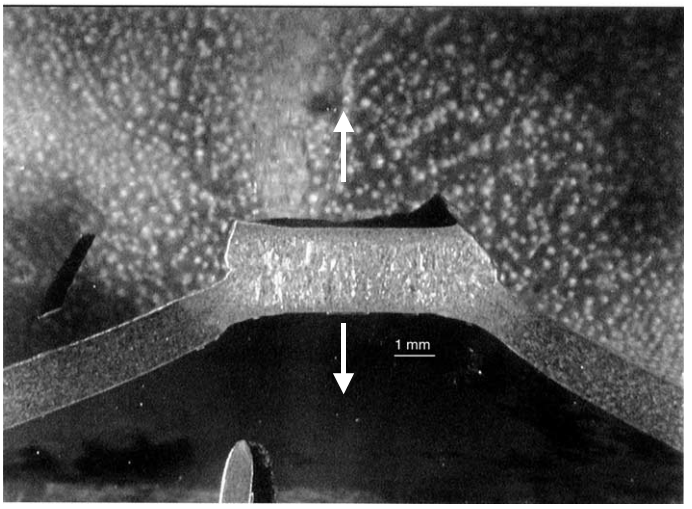

Fig. 8. A micrograph of the cross-section of a failed spot weld in a 1.5 mm specimen under pure opening loading conditions.

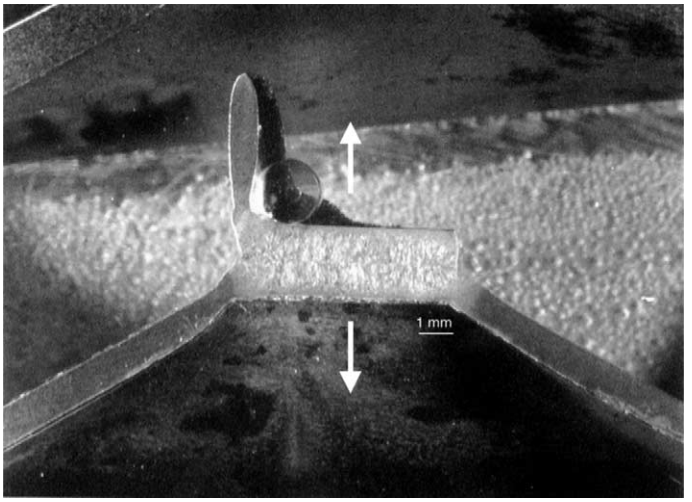

Fig. 9. A micrograph of the cross-section of a failed spot weld in a 1.0 mm specimen under pure opening loading conditions.

diameter. In order to explore the effects of loading conditions or loading angles, the maximum loads recorded from the tests are normalized by the maximum load under pure opening loading conditions for a given sheet thickness. The normalized maximum load, denoted as $\overline{P}$, can be decomposed into the opening and shear components with respect to the spot weld, denoted by $\overline{N}$ and $\overline{S}$, respectively. Normalized opening and shear loads from the experiments for two different thicknesses are shown in Fig. 12. Fig. 12 shows that elliptical curves in terms of $\overline{N}$ and $\overline{S}$ may be possibly used to fit the experimental results. Also, the failure contour for 1.5 mm specimens seems to be smaller. Therefore, we attempt to model the general trends of the maximum loads with consideration of the thickness effect under the combined loads by a lower bound limit load analysis presented in the following section.

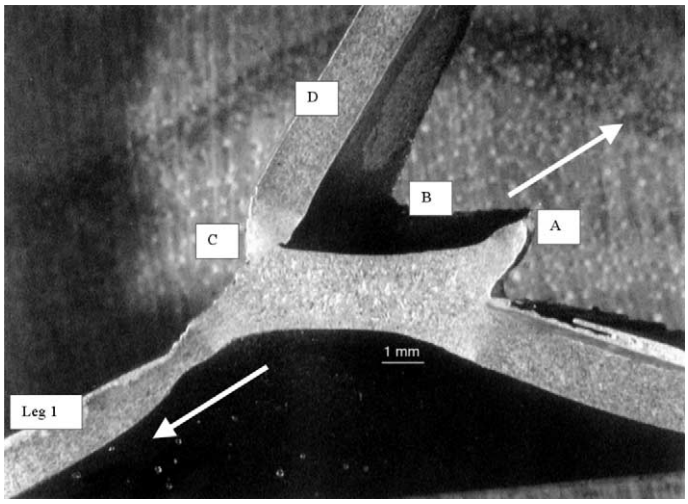

Fig. 10. A micrograph of the cross-section of a failed spot weld in a 1.5 mm specimen under a loading angle of 60°.

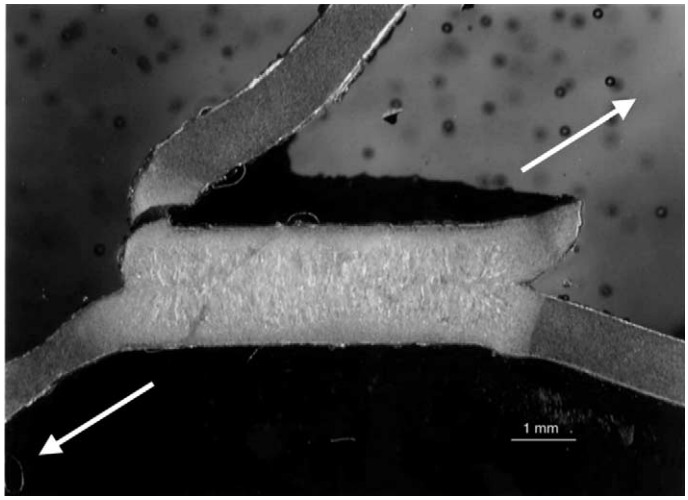

Fig. 11. A micrograph of the cross-section of a failed spot weld in a 1.0 mm specimen under a loading angle of 60°.

4. A lower bound limit load analysis

As discussed earlier, the failure processes of spot welds are quite complex. However, engineering solutions for characterizing the maximum load carrying capacity need to be developed. According to the experimental observations of the failure mechanisms, a lower bound limit load analysis is conducted here under combined opening and shear loading conditions. Note that plastic limit load analysis is commonly used to obtain the maximum load carrying capacity of structures where plastic deformation is extensive at failure, e.g., see Pan (1984, 1986) for limit load analyses of cracked pipes. A comparison of the micrographs shown in Figs. 6, 8–11 suggest that plastic deformation appears extensive near the spot welds at failure. Therefore, a plastic limit load analysis is performed here. For a plastic limit load analysis, rigid perfectly plastic material behavior is first assumed.

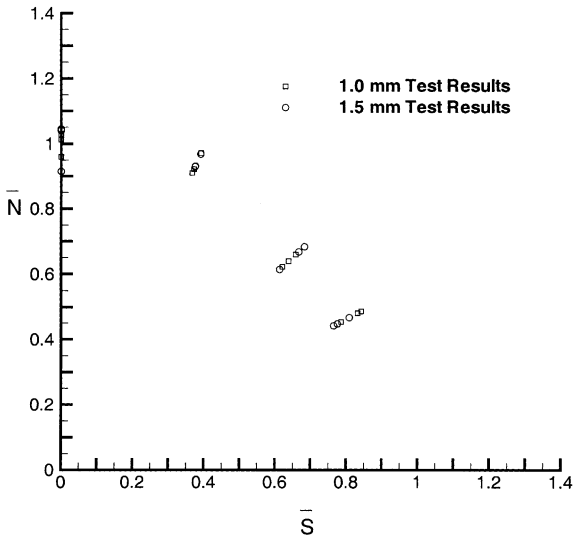

Fig. 12. The normalized opening and shear loads based on the maximum loads from experiments.

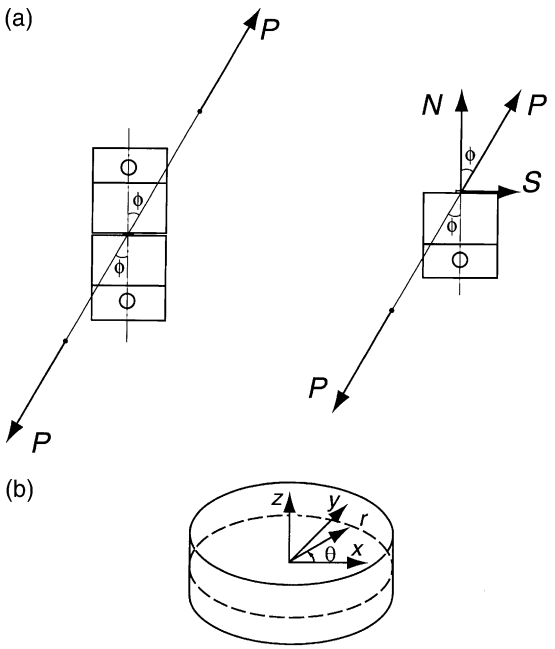

Fig. 13. (a) The resultant load P is resolved into the opening load N and the shear load S, (b) the Cartesian and cylindrical coordinate systems for the idealized cylindrical weld nugget.

Fig. 13(a) shows again a specimen subjected to a remote resultant load P. The resultant load P can be decomposed into the opening load N and the shear load S. For our lower bound limit load analysis, we idealize the weld nugget as a circular cylinder. Fig. 13(b) shows the weld nugget as a circular cylinder and the Cartesian and cylindrical coordinates. The origin of the Cartesian coordinate is located at the center of

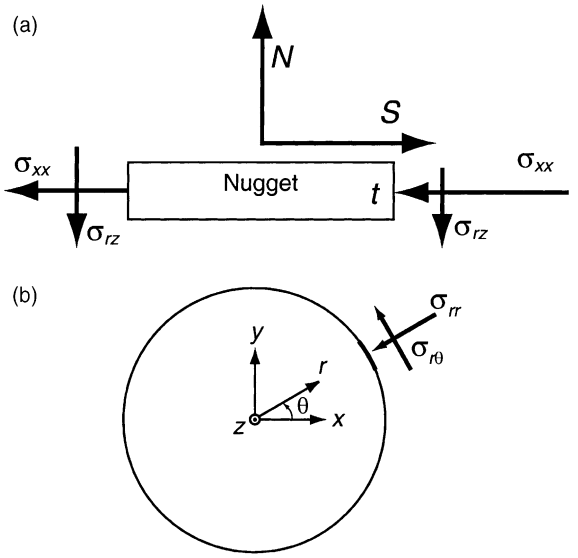

Fig. 14. (a) A side view of the loads and assumed average stresses for the lower part of the weld nugget, (b) a top view of the lower half of the weld nugget.

the weld nugget as shown. For this lower bound analysis, we only consider the lower half of the weld nugget as shown in Fig. 14. For a side view of the nugget shown in Fig. 14(a), the force can be decomposed into two components, N and S, at the center of the nugget. The loads N and S can be balanced by the assumed average stresses on the nugget circumferential surface. Note that in order to develop a lower bound limit load solution, only the equilibrium conditions need to be satisfied. The von Mises yield criterion is employed. Now the stress states along the circumferential surface of the nugget are discussed in the following.

Fig. 14(a) shows a side view of the loads and the assumed average stresses on the circumferential surface of the lower half of the weld nugget. Fig. 14(b) shows a top view of the lower half of the weld nugget with the Cartesian and cylindrical coordinate systems. Fig. 14(b) also shows the stresses σ_{rr} and $\sigma_{r\theta}$ on a surface element along the circumferential surface of the weld nugget. We here assume that the stresses σ_{rr}, $\sigma_{\theta\theta}$ and $\sigma_{r\theta}$ of the material element are derived from the stress state where σ_{xx} is a function of θ and $\sigma_{yy} = \sigma_{xy} = 0$ for the in-plane stresses. Here, σ_{xx} is positive for the left part and negative for the right part of the lower half of the nugget. One can consider the assumed stress state comes from the fact that the shear load S pulls the left part of the adjacent material to nugget and pushes the right part of the adjacent material to the nugget. The stresses on the circumferential surface can now be referred to the cylindrical coordinate system as

$$\sigma_{rr} = \sigma_{xx}(\theta)\cos^2\theta \tag{1}$$

$$\sigma_{r\theta} = \sigma_{xx}(\theta)\sin\theta\cos\theta \tag{2}$$

$$\sigma_{\theta\theta} = \sigma_{xx}(\theta)\sin^2\theta \tag{3}$$

The equilibrium in the x-direction for the lower half of the nugget requires

$$\int_0^{2\pi} (\sigma_{xx}(\theta)\cos\theta) rt\,\mathrm{d}\theta + S = 0 \tag{4}$$

where r is the nugget radius and t is the sheet thickness. Equilibrium in the y-direction is always satisfied since $\sigma_{yy} = \sigma_{xy} = 0$.

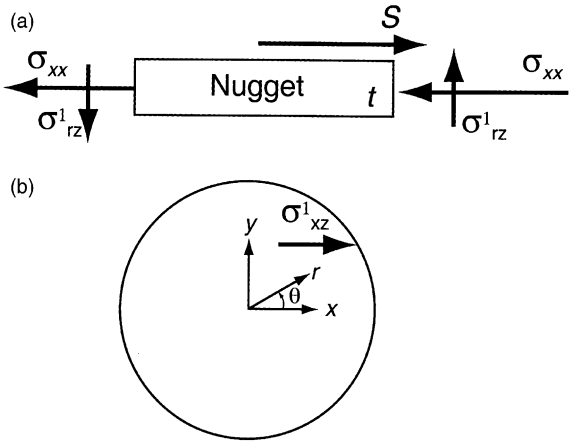

Fig. 15. The shear stress σ^1_{rz} to represent the shear load S. (a) A side view of the lower half of the weld nugget, (b) a top view of the lower half of the weld nugget.

The average stress σ_{xx} through the thickness is assumed to act along the mid-plane of the lower half of the nugget. As shown in Fig. 15(a), average shear stress σ^1_{rz} acting on the circumferential surface of the nugget is needed to balance the moment due to the shear load S and the average stress σ_{xx}. Here, σ^1_{rz} represents the average value of σ_{rz} through the thickness. Now, we are seeking a distribution of σ^1_{rz} as a function of θ. Consider a distribution of σ^1_{xz} to represent the shear load S acting on the top surface of the lower half of the weld nugget as shown in Fig. 15(b). The shear stress can be referred to the cylindrical coordinate system as

$$\sigma^1_{rz} = \sigma^1_{xz}\cos\theta \tag{5}$$

$$\sigma^1_{\theta z} = \sigma^1_{xz}(-\sin\theta) \tag{6}$$

Here, σ^1_{rz} and $\sigma^1_{r\theta}$ represent the components of the shear stress to represent the shear load S. Note that another contribution to the shear stress σ_{rz} due to the opening load N will be discussed later. The moment balance in the y-direction with respect to the lower half of the nugget requires

$$M_y = \int_0^{2\pi} \sigma^1_{rz}(r\cos\theta)tr\,\mathrm{d}\theta - S\frac{t}{2} = 0 \tag{7}$$

when σ^1_{xz} is assumed to be a constant, σ^1_{xz} can be derived as

$$\sigma^1_{xz} = \frac{S}{2\pi r^2} \tag{8}$$

Note that there is no resultant force in the z direction from the distribution of σ^1_{xz} on the circumferential surface of the lower half of the weld nugget.

The opening load N needs to be balanced by another shear stress σ^*_{rz}. Again, σ^*_{rz} represents the average shear stress through the thickness. The equilibrium in the z direction requires

$$N = \int_0^{2\pi} \sigma^*_{rz} rt\,\mathrm{d}\theta \tag{9}$$

Note again that σ^1_{rz} due to the shear load S will not result in any force in the z direction. If we assume that σ^*_{rz} due to N is uniformly distributed along the circumferential surface of the lower half of the weld nugget, the equilibrium in the z direction from Eq. (9) gives

$$\sigma_{rz}^{*} = \frac{N}{2\pi rt} \tag{10}$$

Note that there is no resultant moment due to the constant σ_{rz}^{*} on the circumferential surface of the lower half of the weld nugget. The out-of-plane shear stresses now can be expressed as

$$\sigma_{rz} = \frac{S}{2\pi r^2}\cos\theta - \frac{N}{2\pi rt} \tag{11a}$$

$$\sigma_{\theta z} = -\frac{S}{2\pi r^2}\sin\theta \tag{11b}$$

With the assumption of $\sigma_{zz} = 0$, the von Mises yield criterion can now be expressed as

$$\sigma_{rr}^2 - \sigma_{rr}\sigma_{\theta\theta} + \sigma_{\theta\theta}^2 + 3\sigma_{r\theta}^2 + 3\sigma_{rz}^2 + 3\sigma_{\theta z}^2 = 3\tau_0^2 \tag{12}$$

where τ_0 is the shear yield strength.

We can define the normalized opening and shear loads $\overline{N}$ and $\overline{S}$, respectively, as

$$\overline{N} = \frac{N}{2\pi rt\tau_0} \tag{13}$$

$$\overline{S} = \frac{S}{2\pi rt\tau_0} \tag{14}$$

Based on the assumed stresses as discussed earlier and Eqs. (13) and (14), the von Mises yield criterion for the material elements on the circumferential surface of the lower half of the weld nugget in an average sense can be rewritten as

$$\frac{1}{3}\left(\frac{\sigma_{xx}}{\tau_0}\right)^2 + \overline{N}^2 + \left(\frac{t}{r}\right)^2\overline{S}^2 - 2\overline{N}\left(\frac{t}{r}\right)\overline{S}\cos\theta = 1 \tag{15}$$

Therefore, the lower bound limit load solution in terms of $\overline{N}$ and $\overline{S}$ can be obtained from Eqs. (4) and (15) for any given ratio of t/r. The condition for the existence of a distribution of $\sigma_{xx}(\theta)$ to satisfy Eqs. (4) and (15) for all θ's is discussed in Appendix. The numerical solutions indicate that σ_{xx} has the largest value at $\theta = 0$ and smallest value at $\theta = \pm\pi$. Fig. 16 shows the numerical solutions of $\overline{N}$ and $\overline{S}$ represented by various symbols for $t/r = 0$, 0.313, 0.469, and 0.557. Here, 0.557 is the maximum value of the ratio t/r based on the usual spot welding schedules for low carbon steel sheet metals. Fig. 16 shows that the normalized limit loads or failure contours for spot welds under combined loading conditions are larger for small values of the ratio t/r. Note that, the values of the ratio t/r are 0.313 and 0.469 for 1 mm and 1.5 mm mild steel specimens, respectively. The results for $t/r = 0$ are also plotted. If $t/r = 0$, Eq. (15) becomes

$$\frac{1}{3}\left(\frac{\sigma_{xx}}{\tau_0}\right)^2 + \overline{N}^2 = 1 \tag{16}$$

In order to satisfy the yield criterion, σ_{xx} has to be equal to a constant. When σ_{xx} is equal to a constant, Eq. (4) leads to

$$S = 4rt\sigma_{xx} \tag{17}$$

Combining Eqs. (14), (16) and (17) gives

$$\overline{N}^2 + \frac{\pi^2}{12}\overline{S}^2 = 1 \tag{18}$$

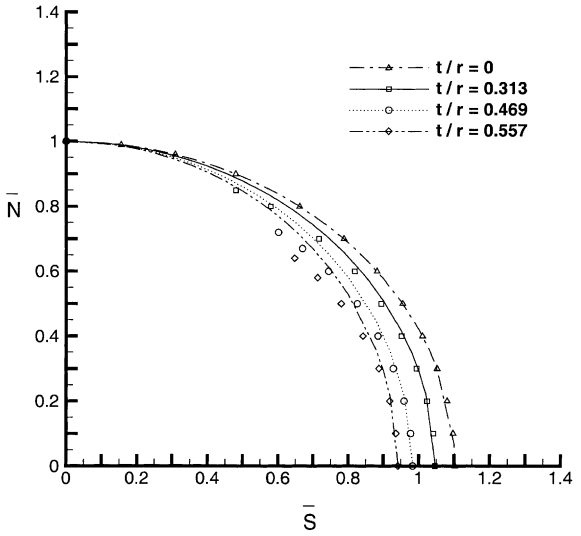

Fig. 16. The lower bound limit load solutions of $\overline{N}$ and $\overline{S}$ for different ratios of t/r. Here, various symbols represent the numerical results based on Eq. (15) with the assumption of σ_{xx} as a function of θ. Various curves represent the numerical results based on Eq. (19) with the assumption of σ_{xx} as a constant.

Hence, the limit load of spot welds for $t/r = 0$ is a quadratic form in nature. Note that when $t/r \neq 0$, the numerical solution does not lead to a quadratic solution anymore.

Since closed-form solutions are usually preferred for engineering applications, we now consider the case where the coupling term of $\overline{N}$ and $\overline{S}$ in Eq. (15) is neglected. In this case, Eq. (15) can be rewritten as

$$\frac{1}{3}\left(\frac{\sigma_{xx}}{\tau_0}\right)^2 + \overline{N}^2 + \left(\frac{t}{r}\right)^2 \overline{S}^2 = 1 \tag{19}$$

Now, σ_{xx} must be assumed as a constant in order to satisfy the yield condition. As before, Eq. (4) leads to

$$S = 4rt\sigma_{xx} \tag{20}$$

Combining Eqs. (19) and (20) leads to

$$\overline{N}^2 + \alpha \overline{S}^2 = 1 \tag{21}$$

where

$$\alpha = \frac{\pi^2}{12} + \left(\frac{t}{r}\right)^2 \tag{22}$$

Eqs. (21) and (22) are plotted as various curves with $t/r = 0$, 0.313, 0.469, 0.557 in Fig. 16. Note that t/r is less than 1. We neglect the coupling term of $\overline{N}$ and $\overline{S}$, which is first order term of t/r, and keep the second order term of t/r in Eq. (15) in order to obtain the closed-form solutions in Eq. (19). As shown in Fig. 16, the solutions without consideration of the coupling term of $\overline{N}$ and $\overline{S}$ give some more overestimation of the limit loads under combined loading conditions as t/r increases. Of course, a non-quadratic equation can be used to fit the numerical solutions more closely. For example,

$$\overline{N}^m + \beta \overline{S}^m = 1 \tag{23}$$

where β is a constant and m is a constant which is different from 2. However, for engineering applications, simple quadratic functions as in Eqs. (21) and (22) should be more convenient to use.

5. Engineering failure criterion for spot welds

Fig. 17 shows the normalized quadratic limit loads or failure contours based on Eqs. (21) and (22) and the normalized maximum loads from experiments. The quadratic failure contours agree well with the experimental results when the normalized shear load is small. However, when the normalized shear load becomes large, the quadratic failure criterion in Eqs. (21) and (22) gives overestimation of the load carrying capacity of spot welds. Of course, a non-quadratic full limit load solution with consideration of the coupling term will give a better fit to the experimental results. Another physical reason to be considered is that the failure mechanisms are different for pure opening and combined loading conditions. The failure occurred near the heat affected zone of the spot weld under near pure opening loading conditions. Under combined loading conditions, the failure initiated at the base metal on the stretching side of the sheet metal. Note that the ultimate tensile strength of the heat affected zone of spot weld is larger than that of the base metal and so is the shear yield strength. If the shear yield strength is larger, the load carrying capacity predicted by a lower bound limit load solution based on plastic shear in the heat affected zone should be higher. Therefore, the limit load solution shows a larger load carrying capacity of spot welds under combined loading conditions.

In order to generate a better engineering failure criterion for spot welds under combined loading conditions, Eq. (21) is modified to fit the experimental results as

$$\overline{N}^2 + \Lambda \overline{S}^2 = 1 \tag{24}$$

where

$$\Lambda = k\left(\frac{\pi^2}{12} + \left(\frac{t}{r}\right)^2\right) \tag{25}$$

Here, we include a correction factor k to fit the experimental results. In this case, k is determined to be 1.29 for both 1.0 and 1.5 mm specimens. From the viewpoint of curve fitting, the values of k should be different for different t/r's. However, k is determined at 1.29 for both the thicknesses possibly due to the relative insensitivity of k for the range of t/r considered here ($t/r = 0.313$ and 0.469 for 1.0 and 1.5 mm specimens).

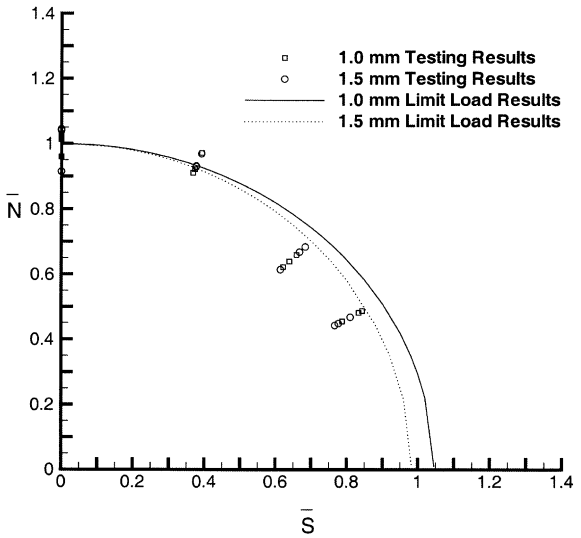

Fig. 17. A comparison of the experimental results and quadratic failure contours obtained from a lower bound limit load analysis.

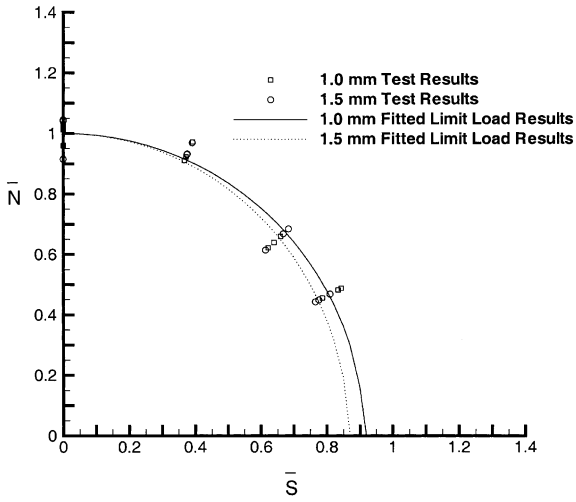

Fig. 18. The experimental results of spot welds under combined opening and shear loads are fitted by the failure quadratic curves.

Λ in Eq. (24) equals to 1.203 and 1.333 for 1.0 and 1.5 mm specimens, respectively, due to the different values of t/r. Note that we have only one correction factor in Eq. (25) because we have experimental data for two thicknesses and one nugget radius. When more experimental data for different r's and t's are available, more correction factors can be introduced to fit the experimental results. Fig. 18 shows the results of the failure criterion based on Eqs. (24) and (25) and the experimental results. The results based on the failure criterion with the correction factor can now fit the experimental results well.

Finally, the normalized resultant load $\overline{P}$ can be obtained from $\overline{N}$ and $\overline{S}$ as

$$\overline{P} = \sqrt{\overline{N}^2 + \overline{S}^2} = \sqrt{\frac{1}{1 + (\Lambda - 1)\sin^2\phi}} \tag{26}$$

where ϕ is the loading angle. Fig. 19 shows $\overline{P}$ as a function of ϕ for $t/r = 0.313$ (for 1.0 mm specimens) and $t/r = 0.469$ (for 1.5 mm specimens) based on Eq. (26). The experimental results are also plotted as symbols in Fig. 19. As shown in the figure, the experimental results appear to agree well with the engineering failure loads based on Eq. (26).

Based on Eq. (26), the maximum loads of mild steel spot welds can be estimated from the tensile strength, sheet thickness and nugget radius. Instead of the nugget diameter directly used in the failure criterion for lap-shear specimens (Heuschkel, 1952), the circumference of the nugget is used in the failure criterion because the loading is supported through the circumferential surface of the nugget. Thus, an engineering failure criterion for spot welds in mild steel sheets can be written based on Eq. (26)

$$P = c_{\tau_0} 2\pi r t \tau_0 \sqrt{\frac{1}{1 + (\Lambda - 1)\sin^2\phi}} \tag{27}$$

Note that τ_0 is the shear yield stress of the base material, c_{τ_0} is a fitting parameter related to the welding processes and geometric parameters, and Λ is a function of the ratio of the sheet thickness to the nugget radius as in Eq. (25). Eq. (27) can be combined with Eq. (25) and rewritten as

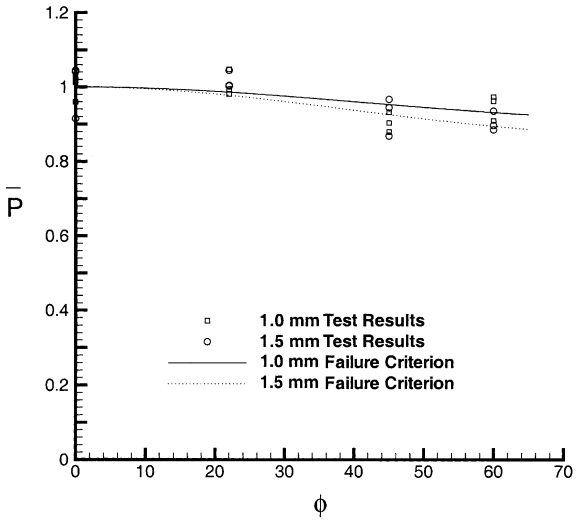

Fig. 19. The normalized maximum load $\overline{P}$ obtained from experiments and the engineering failure criterion for 1.0 and 1.5 mm specimens.

$$P = c_U 2\pi rtU \sqrt{\frac{1}{1 + \left(k\left(\frac{\pi^2}{12} + \left(\frac{t}{r}\right)^2\right) - 1\right)\sin^2\phi}} \tag{28}$$

where c_U is a fitting constant and U is the tensile strength of the base metal. Based on the experimental results in Table 2 and the material properties of the base metal (the 0.2% yield strength is 184.6 MPa (26.78 ksi) and the ultimate tensile strength is 302.3 MPa (43.84 ksi)), c_U is determined to be 1.0036 for the specimens used in this paper. Here, c_U is taken as 1 for simplicity. For example, the failure loads of spot welds for the 1.0 and 1.5 mm sheets can be expressed as

$$P = 2\pi rtU \sqrt{\frac{1}{1 + 0.203\sin^2\phi}} \tag{29}$$

for 1.0 mm specimens and

$$P = 2\pi rtU \sqrt{\frac{1}{1 + 0.333\sin^2\phi}} \tag{30}$$

for 1.5 mm specimens.

6. Conclusions

Failure loads of spot welds under combined opening and shear loads are investigated. Square-cup specimens were used in the experiments to investigate the load carrying capacity of spot welds under combined opening and shear loading conditions. Examination of the micrographs of failed specimens indicates that the failure of spot welds involves crack initiation and growth under fully plastic mixed-mode loading conditions. In order to develop an engineering solution for automotive applications, a lower bound limit load analysis has been performed to understand the effects of the sheet thickness and nugget radius on

the maximum loads, or the failure loads, of spot welds under combined loading conditions. The dependence of the failure loads on the sheet thickness and the nugget radius is expressed in terms of a quadratic function of the ratio of the sheet thickness to the nugget radius. Based on the limit load solution, an engineering failure criterion is proposed to be in quadratic form in terms of the normalized opening and shear loads with consideration of the sheet thickness and the nugget radius under different combined loading conditions.

Acknowledgements

The support of this work for SHL and JP by a contract from Ford Motor Company and a grant from Ford University Research Program is greatly appreciated. The contribution of Dennis Ojemudia of Ford Safety Laboratory to the experiments is also appreciated. In addition, the fabrication of specimens at Ford Pilot Plant and the use of experimental facility at Ford Research Laboratory are appreciated.

Appendix A. Condition for existence of lower bound limit load solution

In order to have a further understanding of the lower bound limit load solution, Eqs. (4) and (15) are closely examined here. From Eqs. (4) and (15), lower bound limit load solutions can be obtained in terms of $\overline{N}$ and $\overline{S}$ for a given ratio of t/r. Under pure opening, pure shear or nearly pure shear loading conditions, Eqs. (4) and (15) can be satisfied for all θ's for a given ratio of t/r. However, under a range of nearly opening loading conditions, Eqs. (4) and (15) may not be satisfied for all θ's.

The distribution of σ_{xx} is examined to understand the reason why lower bound limit load solutions do not exist for nearly opening loading conditions for a given ratio of t/r. Note that, based on Eqs. (4) and (15), σ_{xx} and $\overline{S}$ are simultaneously determined when a normalized opening load $\overline{N}$ and a ratio of t/r are selected. It is possible that a solution of σ_{xx} may not exist for the left part of the lower half of the weld nugget due to the negative value of $\cos\theta$ in Eq. (15). Fig. 20(a) shows the normalized stress σ_{xx}/τ_0 for the lower half of the weld nugget for a given ratio of $t/r = 0.1$. As shown in the figure, the left part $(\pi/2 \leqslant \theta \leqslant 3\pi/2)$ of the weld nugget is under tension and the right part $(-\pi/2 \leqslant \theta \leqslant \pi/2)$ is under compression. Fig. 20(a) shows that the absolute value of σ_{xx}/τ_0 decreases on both the tensile and compressive sides when the normalized opening load $\overline{N}$ increases at a given ratio of t/r. It appears that the maximum absolute value of σ_{xx}/τ_0 occurs at $\theta = 0$ and $\theta = 2\pi$, and the minimum absolute value of σ_{xx}/τ_0 occurs at $\theta = \pi$. When $\overline{N}$ is selected to be 0.982, σ_{xx}/τ_0 is nearly 0 at $\theta = \pi$. However, if $\overline{N}$ is larger than 0.982, a solution of σ_{xx} cannot be found at $\theta = \pi$ for this given ratio of $t/r = 0.1$. Fig. 20(b) shows the normalized stress σ_{xx}/τ_0 for a given normalized opening load $\overline{N} = 0.8$. As shown in the figure, the absolute value of σ_{xx}/τ_0 decreases on the tensile side and increases on the compressive side when the ratio of t/r increases. Here, σ_{xx}/τ_0 is nearly 0 at $\theta = \pi$ when the ratio of t/r is selected to be 0.3679. For the ratio of t/r larger than 0.3679, a solution of σ_{xx} cannot be found at $\theta = \pi$.

As shown in Fig. 20, the existence of solution is determined by the stress state at $\theta = \pi$. Therefore, the stress state at $\theta = \pi$ is examined. When $\theta = \pi$, Eqs. (11a) and (11b) can be rewritten as

$$\sigma_{rz} = -\frac{S}{2\pi r^2} - \frac{N}{2\pi rt} \tag{A.1}$$

$$\sigma_{\theta z} = 0 \tag{A.2}$$

If a solution of σ_{xx} exists ($\sigma_{xx}^2 \geqslant 0$), Eq. (12) leads to

$$\sigma_{rz}^2 \leqslant \tau_0^2 \tag{A.3}$$

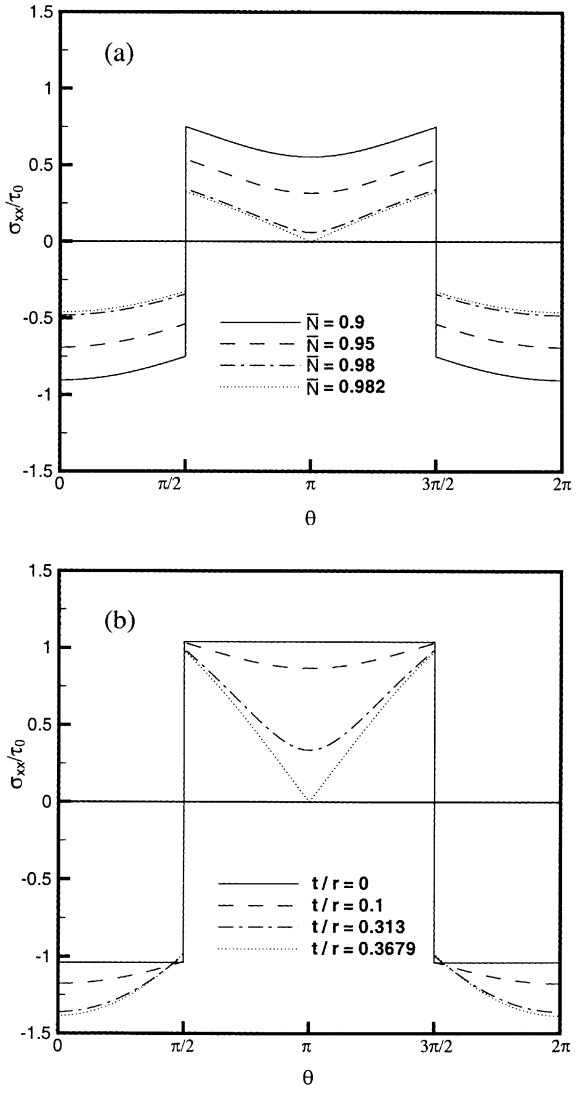

Fig. 20. The normalized stress σ_{xx}/τ_0 on the lower half of the weld nugget: (a) for a fixed ratio of $t/r = 0.1$, (b) for a fixed normalized opening load, $\overline{N} = 0.8$.

Eq. (A.3) can be combined with Eqs. (A.1), (A.2), (13), and (14) as

$$\overline{S}\left(\frac{t}{r}\right) + \overline{N} \leqslant 1 \tag{A.4}$$

The critical condition for the existence of solution appears to be $\sigma_{xx} = 0$ at $\theta = \pi$. In this case, Eq. (A.4) becomes

$$\overline{S}\left(\frac{t}{r}\right) + \overline{N} = 1 \tag{A.5}$$

For a given ratio of t/r, a critical solution corresponds to Eq. (A.5) can be found. The solution is related to a critical loading angle ϕ_c. When the loading angle is less than ϕ_c, a solution cannot be found.

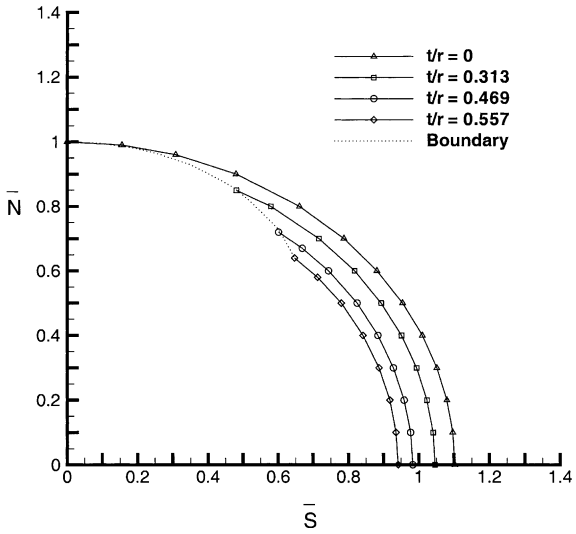

Fig. 21. The limit load solutions and the boundary for the existence of solutions.

Fig. 21 shows the limit load solutions as solid lines for $t/r = 0$, 0.313, 0.469 and 0.577, and the boundary for the existence of solutions as a dotted line. In the figure, the limit load solutions do not exist to the left of the dotted line under nearly opening loading conditions. For $t/r = 0$, the limit load solution is in a quadratic form and a solution can always be found based on Eqs. (4) and (15) for any combinations of opening and shear loads. However, when the value of the ratio of t/r increases from 0, limit load solutions do not exist for nearly opening loading conditions when the loading angle ϕ is less than ϕ_c. The range for no solutions under combined nearly opening loads becomes larger when the ratio of t/r increases. Note that limit load solution always exists under pure opening loading conditions ($\overline{N} = 1$ and $\overline{S} = 0$) for all values of t/r. Fig. 22 shows the critical loading angle ϕ_c, below which a solution does not exist, as a function of t/r. As shown in Fig. 22, the angle ϕ_c increases as t/r increases.

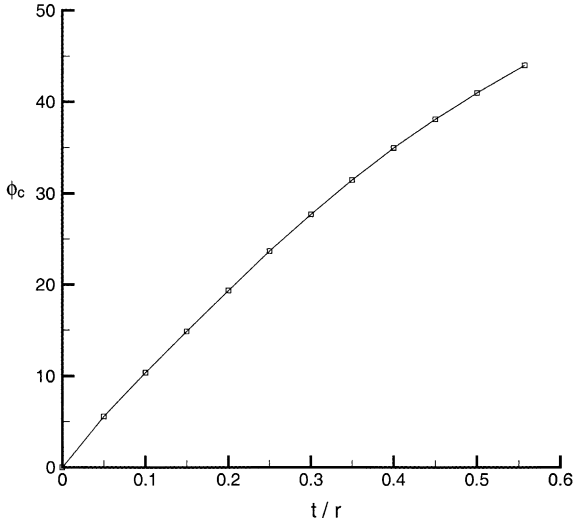

Fig. 22. The critical loading angle ϕ_c as a function of t/r.

References

Davidson, J.A., 1983. A review of the fatigue properties of spot-welded sheet steels. SAE Technical Paper no. 830033, Society of Automotive Engineers, Warrendale, PA.

Ewing, K.W., Cheresh, M., Thompson, R., Kukuchek, P., 1982. Static and impact strengths of spot welded HSLA and low carbon steel joints. SAE Technical Paper no. 820281, Society of Automotive Engineers, Warrendale, PA.

Hartmann, E.C., 1958. Mechanical tests of spot welds. Welding Journal 37, 520–523.

Heuschkel, J., 1952. The expression of spot-weld properties. Welding Journal 31, 931–943.

Lee, Y.-L., Wehner, T.J., Lu, M.-W., Morrissett, T.W., Pakalnins, E., 1998. Ultimate strength of resistance spot welds subjected to combined tension and shear. Journal of Testing and Evaluation 26, 213–219.

Pan, J., 1984. Some considerations on estimation of energy release rates for circumferentially cracked pipes. ASME Journal of Pressure Vessel Technology 106, 391–398.

Pan, J., 1986. Estimation of energy release rates and instability analysis for a pipe with a circumferential surface crack subjected to bending. ASME Journal of Pressure Vessel Technology 108, 33–40.

Radaj, D., 1989. Stress singularity, notch stress and structural stress at spot-welded joints. Engineering Fracture Mechanics 34, 495–506.

Sawhill, J.M., Furr, S.T., 1981. Spot weldibility tests for high-strength steels. SAE Technical Paper no. 810352, Society of Automotive Engineers, Warrendale, PA.

Sheppard, S.D., Pan, N., 2001. A look at fatigue: is resistance spot welds-notch or crack? SAE Technical Paper no. 2001-01-0433, Society of Automotive Engineers, Warrendale, PA.

Swellam, M.H., Banas, G., Lawrence, F.V., 1994. A fatigue design parameter for spot welds. Fatigue and Fracture of Engineering Materials and Structures 17, 1197–1204.

VandenBossche, D.J., 1977. Ultimate strength and failure mode of spot welds in high strength steels. SAE Technical Paper no. 770214, Society of Automotive Engineers, Warrendale, PA.

Wang, P.-C., Ewing, K.W., 1991. Fracture mechanics analysis of fatigue resistance of spot welded coach-peel joints. Fatigue and Fracture of Engineering Materials and Structures 14, 913–930.

Wung, P., 2001. A force-based failure criterion for spot weld analysis. Journal of Experimental Mechanics 41, 107–113.

Wung, P., Stewart, W., 2001. Method of analyzing spot welded structures. Patent no. US 6,186,011 B1.

Wung, P., Walsh, T., Ourchane, A., Stewart, W., Jie, M., 2001. Failure of spot welds under in-plane static loading. Journal of Experimental Mechanics 41, 100–106.

Zhang, S., 2001. Recent developments in analysis and testing of spot welds. SAE Technical Paper no. 2001-01-0432, Society of Automotive Engineers, Warrendale, PA.

Zuniga, S., Sheppard, S.D., 1997. Resistance spot weld failure loads and modes in overload conditions. In: Piascik, R.S., Newman, J.C., Dowling, N.E. (Eds.), Fatigue and Fracture Mechanics, ASTM STP 1296, American Society for Testing and Materials, West Conshohocken, PA, pp. 469–489.